Bioorganic Chemistry 93 (2019) 103335

Contents lists available at ScienceDirect

Bioorganic Chemistry

journal homepage: www.elsevier.com/locate/bioorg

# Design, synthesis and biological evaluation of oxygenated chalcones as potent and selective MAO-B inhibitors

Della Grace Thomas Parambi[a,1], Jong Min Oh[b,1], Seung Cheol Baek[b], Jae Pil Lee[b], Anna Rita Tondo[c], Orazio Nicolotti[d], Hoon Kim[b,*], Bijo Mathew[e,*]

[a] Department of Pharmaceutical Chemistry, Jouf University, Sakaka, Al Jouf 2014, Saudi Arabia
[b] Department of Pharmacy, and Research Institute of Life Pharmaceutical Sciences, Sunchon National University, Suncheon 57922, Republic of Korea
[c] Istituto di Ricerche Farmacologiche Mario Negri IRCCS, Via la Masa 19, 20156 Milano, Italy
[d] Dipartimento di Farmacia—Scienze del Farmaco, Università degli Studi di Bari "Aldo Moro", via E. Orabona, 4, I-70125 Bari, Italy
[e] Division of Drug Design and Medicinal Chemistry Research Lab, Department of Pharmaceutical Chemistry, Ahalia School of Pharmacy, Palakkad 678557, Kerala, India

ARTICLE INFO

*Keywords:*
Chalcone
MAO inhibition
Kinetics
Reversibility
Molecular docking

ABSTRACT

The present study documents the synthesis of oxygenated chalcone (**O1–O26**) derivatives and their abilities to inhibit monoamine oxidases. All 26 derivatives examined showed potent inhibitory activity against MAO-B. Compound **O23** showed the greatest inhibitory activity against MAO-B with an $IC_{50}$ value of 0.0021 μM, followed by compounds **O10** and **O17** ($IC_{50}$ = 0.0030 and 0.0034 μM, respectively). In addition, most of the derivatives potently inhibited MAO-A and **O6** was the most potent inhibitor with an $IC_{50}$ value of 0.029 μM, followed by **O3**, **O4**, **O9**, and **O2** ($IC_{50}$ = 0.035, 0.053, 0.072, and 0.082 μM, respectively). **O23** had a high selectivity index (SI) value for MAO-B of 138.1, and **O20** ($IC_{50}$ value for MAO-B = 0.010 μM) had an extremely high SI of > 4000. In dialysis experiments, inhibitions of MAO-A and MAO-B by **O6** and **O23**, respectively, were recovered to their respective reversible reference levels, demonstrating both are reversible inhibitors. Kinetic studies revealed that **O6** and **O23** competitively inhibited MAO-A and MAO-B, respectively, with respective $K_i$ values of 0.016 ± 0.0007 and 0.00050 ± 0.00003 μM. Lead compound are also non-toxic at 200 μg/mL in normal rat spleen cells. Molecular docking simulations and subsequent Molecular Mechanics/Generalized Born Surface Area calculations provided a rationale that explained experimental data.

## 1. Introduction

Monoamine oxidases (MAOs) are major metabolizing enzymes and attractive target for the treatment of neurodegenerative disorders. MAOs are composed of a flavin adenine dinucleotide (FAD) covalently bound to a cysteine residue, and therapeutics that inhibit these enzymes are viewed as serious contenders for future therapy [1]. MAOs are vital for the deamination, and thus, for regulations of the levels of biogenic amines like neuroamines, xenobiotic amines (e.g., monoamine neurotransmitters), hormones, and exogenous amines present in peripheral tissues and brain [2]. MAOs have been studied extensively and are composed of two isoenzymes, that is, MAO-A and MAO-B, which are both associated with the mitochondrial outer-membrane and exhibit different substrate specificities, inhibitor sensitivities, and tissue localizations. Both isoenzymes are encoded on the X chromosome by different genes [3], and are present in variable quantities in human tissues [4]. An elaborate study on the kinetics of MAOs illustrated that the reaction pathways of MAO-A and B differ and that this difference may depend upon the substrate used and their sources [5].

MAOs crucially modulate the functions of neurotransmitters, and thus, are of interest for the treatment of depression and various neurodegenerative disorders [6]. Oxidative deamination by MAOs can diminish levels of neurotransmitters in nerve terminals, but this process generates free radicals, hydrogen peroxide, and reactive oxygen species (ROS) [7], which can cause protein disruption, mitochondrial dysfunction, neuronal apoptosis, lipid peroxidation, and eventually neuron death. Accordingly, the design and development of specific drug candidates that inhibit the two isoforms of MAO have considerable therapeutic potential [8]. Selective inhibitors of MAO-A are considered to be members of the third line treatment arsenal for anxiety and depression, whereas MAO-B inhibitors have been demonstrated to be effective treatments for neurodegenerative diseases such as Alzheimer's

* Corresponding authors.
*E-mail addresses:* hoon@sunchon.ac.kr (H. Kim), bijo.mathew@ahalia.ac.in (B. Mathew).
[1] Authors contributed equally.

https://doi.org/10.1016/j.bioorg.2019.103335
Received 3 August 2019; Received in revised form 30 September 2019; Accepted 2 October 2019
Available online 03 October 2019
0045-2068/ 

disease (AD) and Parkinson's disease [9,10]. Many oxygen-containing scaffolds like coumarin and chromone have attracted considerable attention because of their abilities to inhibit both MAO isoforms [11–18].

Recently chalcone scaffolds have been shown to provide a basis for inhibiting MAOs [19–27]. The relevance of the chalcone scaffold as a privileged structure in medicinal chemistry has been highlighted in a very recent review [28,29]. Despite of the disadvantages of chalcone scaffold for capable of forming irreversible bonds with other molecules, resulting in toxic effects, such as allergenic reactions, mutagenicity, and carcinogenicity, many promising candidates from these family have been extensively researched and patented till now [30,31].

Moreover it is further proved when browsing ChEMBLdb, a large collection of 611333 small molecules provided with high quality experimental bioactivity data [32]. By using the chalcone scaffold as a query in target prediction program such as the recent MuSSel, a publicly available platform upon the request of a free license [33–35]. Results are enclosed as supporting information.

Decorating heterocycles with diverse functional groups around the α, β-unsaturated linker of chalcone has revealed some fascinating chemistry [36]. Reports issued on the topic show many α, β-unsaturated scaffolds selectively inhibit MAO-B rather than MAO-A [37–39], and that this selectivity difference depends upon the nature and orientation of various electron donating and withdrawing motifs on the phenyl system of chalcone scaffolds. By introducing various electron donating and withdrawing groups on the phenyl ring or the hetero cycle participation around the three carbon enone system, a new class of reversible and selective chalcone-based MAO-B inhibitors has been identified. The presence of dimethylamino, ethyl, bromo, or chloro groups at the *para* position of the phenyl **A** ring of chalcone are associated with pronounced MAO-B inhibition, and it has been hypothesized that these lipophilic groups are efficiently accommodated by the hydrophobic region of the entrance cavity of MAO-B [40–47]. Recently our group also examined the bio-distributions of potent chalcone based MAO-B inhibitors and found that molecules that bind more strongly with human serum albumin (HAS) have better inhibitory characteristics [48,49]. In the present study, we prepared 26 oxygenated chalcones and investigated their MAO inhibitory profiles and structure activity relationships (SARs), especially the importance of the number of alkyl groups between the two oxygen atoms in the **A** ring and the effect of various groups on the **B** ring. The study mainly highlighted the importance of metheynedioxy (MDO) and ethylenedioxy (EDO) ring in the chalcone scaffold towards MAO inhibition.

## 2. Result and discussion

### 2.1. Chemistry

Chalcones (**O1–O26**) were prepared by the Claisen-Schmidt condensation of 1-(2*H*-1,3-benzodioxol-5-yl)ethan-1-one and 1-(2,3-dihydro-1,4-benzodioxin-6-yl)ethan-1-one in the presence of various aryl substituted benzaldehydes in basic alcoholic medium (refer to Scheme 1). All synthesized compounds were characterized by $^{1}$H NMR, $^{13}$C NMR, and mass spectrometry. Large coupling constants (15 Hz) showed that the double bonds of chalcones were in the *trans* configuration [50]. Spectra are available in Supplementary materials.

### 2.2. Biological evaluation

#### 2.2.1. MAO inhibition studies

All 26 derivatives showed potent inhibitory activity against MAO-B at 10 μM with residual activities of < 30% and most derivatives showed little residual activity (Table 1). Compound **O23** inhibited MAO-B most with an $IC_{50}$ value of 0.0021 μM, followed by **O10** and **O17** ($IC_{50}$ = 0.0030 and 0.0034 μM, respectively). Interestingly compound **O23** inhibited MAO-B 21 times more potently than the selective, reversible MAO-B inhibitor lazabemide ($IC_{50}$ = 0.046 μM) and 11 times more potently than the irreversible MAO-B inhibitor pargyline (0.023 μM), which were used as reference compounds in the current study. Compounds **O20**, **O21**, **O22, O2**, **O3**, **O4**, **O7**, **O14**, **O24**, and **O26** also potently inhibited MAO-B with the $IC_{50}$ values ranging from 0.013 to 0.018 μM and were more potent than the references. The other compounds inhibited MAO-B with $IC_{50}$ values ranging from 0.021 to 0.068 μM. Regarding selectivity indices (SIs), **O23** showed a high value for MAO-B at 138.1, while **O10** and **O17** had lower values (43.3 and 102.9, respectively) (Table 1). Compound **O20** ($IC_{50}$ value for MAO-B = 0.010 μM) had an extremely high SI of > 4000.

In addition, most of the compounds potently inhibited MAO-A at 10 μM by > 50%, except compounds **O15** and **O20** (Table 1). Compound **O6** inhibited MAO-A most with an $IC_{50}$ value of 0.029 μM, followed by **O3**, **O4**, **O9**, and **O2** ($IC_{50}$ = 0.035, 0.053, 0.072, and 0.082 μM, respectively). Compound **O6** inhibited MAO-A 32 times more potently than toloxatone (a MAO-A inhibitor; $IC_{50}$ = 0.93 μM) in a non-selective manner, which offers an advantage as its low SI can be utilized to treat the depressive symptoms associated with PD [51]. Compounds **O1**, **O5**, **O7**, **O8**, **O10**, **O17**, and **O23** also effectively inhibited MAO-A with $IC_{50}$ values ranging from 0.13 to 0.35 μM.

#### 2.2.2. Structure activity relationships (SARs) of chalcones with respect to MAO inhibition

Considering the inhibitory profile of diverse oxygenated chalcones used in the study, most of the compounds were selective for MAO-B inhibition, but the compounds with potent MAO-A inhibitory activity were non-selective. We mainly focused on the effects of (a) the number of alkyl groups between the two oxygen atoms in the **A** ring, and (b) of the various electron donating withdrawing groups and their orientations in the **B** ring. Increasing the number of alkyl groups between the two oxygen atoms improved MAO-B inhibition and selectivity. Analogs with an ethylenedioxy ring on **A** ring tended to enhance selectivity for MAO-B. The presence of fluorine atom at *para* position of phenyl ring **B** resulted in the greatest MAO-B inhibition (**O23** and **O10**), and shifting fluorine from *para* to *meta* or *ortho* (**O24** and **O25**) of ethylenedioxy chalcones reduced MAO-B inhibition but increased selectivity. Introduction of a nitro group (electron withdrawing) at the *para* position of ring **B** (**O20**) resulted in the highest selectivity (SI > 4000) with a low $IC_{50}$ value (0.010 μM) for MAO-B. Introduction of an ethyl group in methylenedioxy chalcone (**O6**) resulted in a high level of non-selective MAO-A inhibition. Introduction of methyl group on the *para* position of ring **B** on EDO containing chalcone (**O17**) leads to an increasing MAO-B potency, suggesting that methyl group is as good as -F atom. The SAR concluded that presence of EDO unit have greater impact than the MDO in the chalcone scaffold for both potency and selectivity on MAO-B inhibition. An overview of the SARs of oxygenated chalcones with respect to MAO inhibition is provided in Fig. 1.

#### 2.2.3. Kinetics

Kinetic studies were conducted on MAO-A inhibition by **O6** and MAO-B inhibition by **O23**. Lineweaver-Burk plots and secondary plots showed **O6** competitively inhibited MAO-A with a $K_i$ value of 0.016 ± 0.0007 μM (Fig. 2A&B), indicating **O6** potently, reversibly, and competitively inhibited MAO-A. MAO-B inhibition by **O23** was competitive with a $K_i$ value of 0.00050 ± 0.00003 μM (Fig. 2C&D), which suggests **O23** bound to the active site of free MAO-B and that it acted as a potent, selective, and competitive inhibitor.

#### 2.2.4. Reversibility

Reversibility studies on the inhibitions of MAO-A and MAO-B were conducted using **O6** and **O23**, respectively. Their relative activities of un-dialyzed ($A_U$) and dialyzed ($A_D$) samples were calculated. In these experiments, inhibition of MAO-A by **O6** was recovered from 46.9% (value of $A_U$) to 88.2% (value of $A_D$), and this recovery was similar to that observed for toloxatone (the reversible reference) (from 33.6 to 89.7%) (Fig. 3A). Inhibition of MAO-B by **O23** recovered from 26.9%

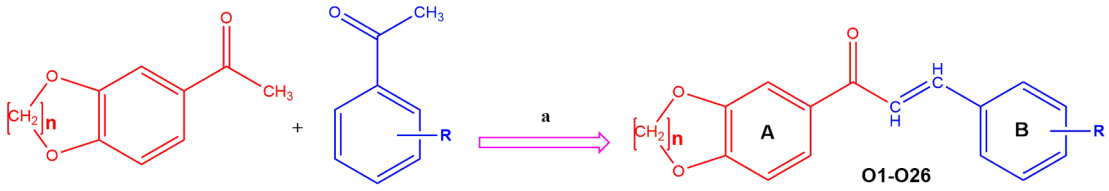


| Code | n | R | Code | n | R |
|---|---|---|---|---|---|
| O1 | 1 | H | O14 | 2 | H |
| O2 | 1 | 4-OH | O15 | 2 | 4-OH |
| O3 | 1 | 4-$OCH_3$ | O16 | 2 | 4-$OCH_3$ |
| O4 | 1 | 4-$CH_3$ | O17 | 2 | 4-$CH_3$ |
| O5 | 1 | 4-$N(CH_3)_2$ | O18 | 2 | 4-$N(CH_3)_2$ |
| O6 | 1 | 4-$C_2H_5$ | O19 | 2 | 4-$C_2H_5$ |
| O7 | 1 | 4-$NO_2$ | O20 | 2 | 4-$NO_2$ |
| O8 | 1 | 4-Cl | O21 | 2 | 4-Cl |
| O9 | 1 | 4-Br | O22 | 2 | 4-Br |
| O10 | 1 | 4-F | O23 | 2 | 4-F |
| O11 | 1 | 3-F | O24 | 2 | 3-F |
| O12 | 1 | 2-F | O25 | 2 | 2-F |
| O13 | 1 | 4-$CF_3$ | O26 | 2 | 4-$CF_3$ |

**a = Reagents and condition: 40%KOH/$C_2H_5OH$-10hr stirr**

**Scheme 1.** Synthetic route used to produce the 26 oxygenated chalcones.

(value of $A_U$) to 90.9% (value of $A_D$), and the recovery was similar to that of lazabemide (the reversible reference) (from 39.8 to 91.9%) (Fig. 3B). Inhibitions of MAO-A and MAO-B by the irreversible inhibitors, clorgyline and pargyline, respectively, were not recovered. These experiments showed inhibitions of MAO-A and MAO-B by **O6** and **O23**, respectively, were recovered to respective reversible reference levels, showing both acted as reversible inhibitors (see Fig. 4).

### 2.2.5. Cytotoxicity

Short term *in vitro* cytotoxicity studies were performed by Trypan blue dye exclusion test in the rat spleen cells. The percentage of cell death was found to be 4 and 11% at 200 μg/mL for the most potent MAO-B inhibitors **O23** and **O10** respectively. The details of the cytotoxicity studies were shown in Table 2.

## 2.3. Computational studies

**O10** and **O23**, which exhibited outstanding inhibitory activity against MAO-B, were docked into the X-ray identified binding sites of MAO-A (PDB code: 2Z5X) and MAO-B (PDB code: 2V5Z) as previously described [52]. In addition, docking scores and binding free energies were calculated (refer to Table 3). The docking score values of the two compounds were close to that of the X-ray cognate ligand (i.e., Safinamide) of MAO-B (−11.087 kcal/mol) [53]. Interestingly, a significant energy gap between the docking scores of **O10** and **O23** with MAO-A and that of the X-ray cognate ligand (i.e., Harmine) (−10.032 kcal/mol) of MAO-A was found.

Of the two lead compounds, that are **O10** and **O23**, the latter was nearest the FAD unit in the inhibitor binding cavity of MAO-B and showed stronger π-π stacking interactions between its benzoxolane moiety and Y435, Y398, and I199 of MAO-B. Noteworthy, the Y326 to I335 mutation observed when comparing active site residues of MAO-B and MAO-A is very much relevant for molecular selectivity. As shown in Fig. 4, Y326 plays a key role for selectivity by establishing a potential hydrogen bond with hydrogen bond acceptor groups of partner ligands **O10** and **O23**. Notably, the relevance of Y326 in modulating selectivity was further observed when docking **O6**, which is provided with moderate inhibition but very low selectivity ($IC_{50}$, MAO-A = 0.029 mM; $IC_{50}$, MAO-B = 0.027 μM). Further details are reported as Supporting Information. In addition, binding free energy analyses indicated that binding affinities of **O23** and **O10** with MAO-B were greater than that observed for MAO-A. In-line with experimentally determined inhibition and SI values, MM-GBSA calculations returned a higher binding free energy for **O23** than **O10**.

Rotation through 180° allows **O23** to adopt two binding conformations (Fig. 5), which might explain the higher experimental SI of **O23** for MAO-A. As shown on the right-hand side of Fig. 5, O23 shows the expected binding topology (that is the benzodioxane ring facing the FAD) only paying a higher energetic cost (−8.061 kcal/mol versus −8.593 kcal/mol) because of the steric hindrance of Y407 and Y444.

**Table 1**
Inhibition of recombinant human MAO enzymes by oxygenated chalcones.[a]

| Compounds | Residual activity at 10 μM (%) | | $IC_{50}$ (μM) | | SI[b] |
|---|---|---|---|---|---|
| | MAO-A | MAO-B | MAO-A | MAO-B | |
| O1 | 4.30 ± 2.35 | −1.47 ± 3.46 | 0.31 ± 0.0026 | 0.026 ± 0.0030 | 11.9 |
| O2 | 13.1 ± 1.14 | 1.47 ± 0.52 | 0.082 ± 0.036 | 0.015 ± 0.0025 | 5.47 |
| O3 | −3.97 ± 2.82 | −6.62 ± 2.71 | 0.035 ± 0.0057 | 0.015 ± 0.0037 | 2.33 |
| O4 | 0.33 ± 1.40 | −6.25 ± 0.65 | 0.053 ± 0.0052 | 0.013 ± 0.0037 | 4.08 |
| O5 | 2.64 ± 0.01 | 6.62 ± 8.12 | 0.31 ± 0.031 | 0.045 ± 0.0014 | 0.69 |
| O6 | −2.32 ± 0.50 | −4.04 ± 2.9 | 0.029 ± 0.010 | 0.027 ± 0.0006 | 1.07 |
| O7 | 16.4 ± 5.59 | −4.59 ± 1.48 | 0.18 ± 0.0022 | 0.014 ± 0.00001 | 12.9 |
| O8 | 5.30 ± 2.34 | −1.42 ± 2.01 | 0.15 ± 0.0070 | 0.024 ± 0.00036 | 6.25 |
| O9 | 0.36 ± 0.52 | −2.82 ± 0.99 | 0.072 ± 0.021 | 0.021 ± 0.0012 | 3.43 |
| O10 | 4.70 ± 3.55 | −3.18 ± 1.48 | 0.13 ± 0.020 | 0.0030 ± 0.0009 | 43.3 |
| O11 | 37.3 ± 1.26 | −6.72 ± 0.53 | 1.93 ± 0.046 | 0.029 ± 0.00031 | 66.6 |
| O12 | 3.52 ± 0.19 | −8.49 ± 2.04 | 1.25 ± 0.0049 | 0.027 ± 0.0035 | 46.3 |
| O13 | 6.24 ± 3.77 | −11.0 ± 1.55 | 1.43 ± 0.014 | 0.024 ± 0.0047 | 59.6 |
| O14 | 41.1 ± 3.94 | −3.7 ± 2.05 | 5.88 ± 1.40 | 0.018 ± 0.0022 | 326.7 |
| O15 | 59.6 ± 1.60 | 27.8 ± 3.25 | 24.9 ± 4.18 | 0.068 ± 0.017 | 366.2 |
| O16 | 17.5 ± 2.38 | −3.7 ± 3.09 | 1.54 ± 0.22 | 0.025 ± 0.0020 | 61.6 |
| O17 | −9.31 ± 5.23 | −29.3 ± 1.92 | 0.35 ± 0.030 | 0.0034 ± 0.0011 | 102.9 |
| O18 | 38.0 ± 1.12 | 7.3 ± 2.03 | 6.10 ± 0.059 | 0.032 ± 0.0061 | 190.6 |
| O19 | 17.1 ± 2.44 | −4.4 ± 2.05 | 0.74 ± 0.068 | 0.025 ± 0.0032 | 29.6 |
| O20 | 74.0 ± 7.23 | −6.37 ± 2.95 | > 40 | 0.010 ± 0.0040 | > 4,000 |
| O21 | −1.34 ± 7.33 | −12.8 ± 1.88 | 1.31 ± 0.013 | 0.010 ± 0.0013 | 131.0 |
| O22 | 7.38 ± 3.54 | −14.2 ± 1.86 | 0.94 ± 0.069 | 0.010 ± 0.0052 | 94.0 |
| O23 | 22.9 ± 4.46 | −8.86 ± 1.42 | 0.29 ± 0.0069 | 0.0021 ± 0.00012 | 138.1 |
| O24 | 46.8 ± 2.47 | 2.47 ± 2.48 | 10.18 ± 1.07 | 0.013 ± 0.0023 | 783.1 |
| O25 | 42.9 ± 0.81 | −7.08 ± 1.93 | 12.58 ± 1.39 | 0.036 ± 0.00053 | 349.4 |
| O26 | 43.4 ± 0.81 | −8.85 ± 3.42 | 8.39 ± 0.37 | 0.015 ± 0.0017 | 559.3 |
| Toloxatone[c] | – | – | 0.93 ± 0.027 | > 80 | |
| Lazabemide | – | – | > 80 | 0.046 ± 0.0048 | |
| Clorgyline | – | – | 0.0057 ± 0.00045 | 2.23 ± 0.21 | |
| Pargyline | – | – | 3.07 ± 0.17 | 0.023 ± 0.0041 | |

[a] Results are expressed as the means ± standard errors of duplicate experiments.
[b] SI values are expressed for MAO-B versus MAO-A.
[c] For reference compounds, inhibitory activities were determined after preincubating them with enzymes for 30 min.

*2.3.1. In silico prediction of ADME/Tox properties*

Finally, we carried out further in silico investigations on compounds **O10** and **O23**. First, we calculated a long list of pharmaceutically relevant properties by using QikProp Base a quick, accurate, easy-to-use absorption, distribution, metabolism, and excretion (ADME) prediction program designed by Professor William L. Jorgensen [54]. Based on this analysis, we observed that that both **O10** and **O23** explored physicochemical properties experienced by the 95% of known drugs. For instance, the predicted brain/blood partition coefficient is equal to 0.051 and 0.030 for **O10** and **O23**, respectively, being the recommended range for orally delivered drugs to cross the blood-brain barrier between −3.00 and l.2. For the sake of completeness, comprehensive spectra of all the predicted properties are enclosed in a file available as Supplementary Materials.

## 3. Conclusion

The current study documents the synthesis of and the results of MAO inhibition studies on a diverse class of chalcones (**O1–O26**) containing methylenedioxy and ethylenedioxy rings. Most of the chalcones containing an ethylenedioxy ring exhibited potent and highly selective MAO-B inhibition. The representative compounds **O23, O10,** and **O17** potently inhibited MAO-B with $IC_{50}$ values of 0.0021, 0.0030, and 0.0034 μM, respectively, and did so more effectively than the reference inhibitors, lazabemide and pargyline ($IC_{50}$ values of 0.046 and 0.023 μM, respectively). Compound **O6** inhibited MAO-A 32 times more than toloxatone (the reference inhibitor; $IC_{50}$ = 0.93 μM) but in a non-selective manner. In the SAR study, we focused on the effects of the number of alkyl groups between the two oxygen atoms of the chalcone **A** ring and of different groups on the phenyl **B** ring. Interestingly, the *in vitro* cytotoxic studies results show that **O23** and **O10** is nontoxic at 200 μg/ml with 4% and 11% of percentage of death cells. Based on the inhibitory data obtained, we conclude chalcone derivatives offer a means of discovering novel MAO inhibitors. Furthermore, our results raise the possibility of developing reversible MAO inhibitors that might provide safer MAO-inhibitor based therapies. We will study further *in vivo* analysis about the levels of biogenic amines in near future by using these compounds.

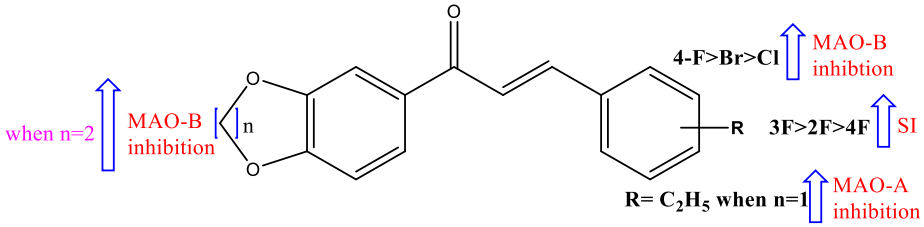


**Fig. 1.** SARs of oxygenated chalcones towards MAO inhibition.

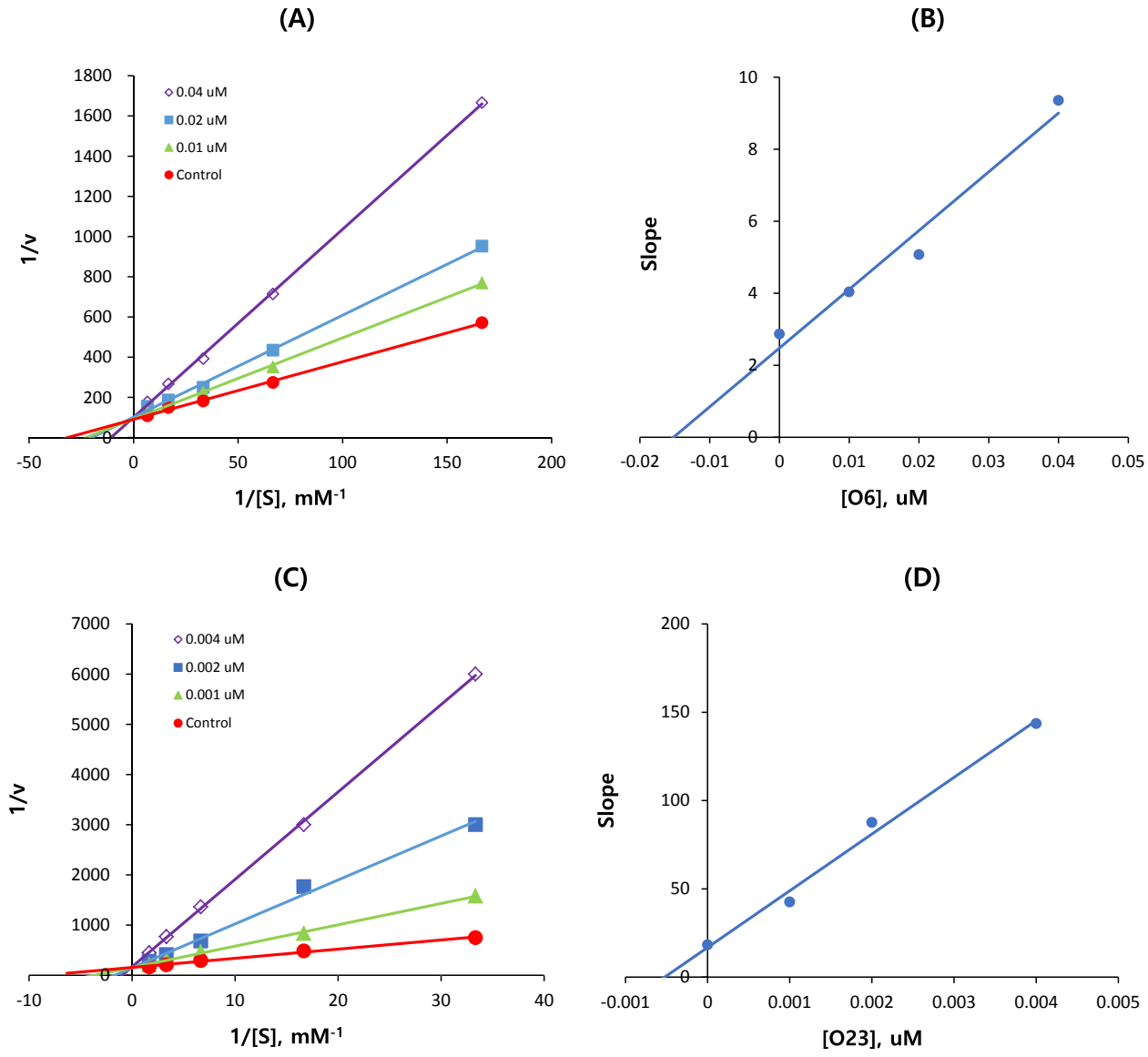


**Fig. 2.** Lineweaver-Burk plots for MAO-A and MAO-B inhibitions by O6 (A) and O23 (C), respectively, and their respective secondary plots (B) and (D) of the slopes vs. inhibitor concentrations.

## 4. Materials and methods

### 4.1. Synthesis

Equimolar quantities of substituted benzaldehyde and 1-(2*H*-1,3-benzodioxol-5-yl)ethan-1-one or 1-(2,3-dihydro-1,4-benzodioxin-6-yl) ethan-1-one were dissolved in 40% KOH and ethanol. The reaction mixture was then stirred for 10 h and poured into ice-cold water. The precipitated product was washed with water, dried, and recrystallized from ethanol.

#### 4.1.1. (2E)-1-(2H-1,3-benzodioxol-5-yl)-3-phenylprop-2-en-1-one (O1)

Yield: 70%. $^{1}$H NMR (500 MHz, $CDCl_3$)δ: 6.07 (s, 2H, O-$CH_2$-O), 6.91–6.89 (d, 1H, *J* = 10.0 Hz, -ArH), 7.43–7.41, (d, 3H, *J* = 10.0 Hz, -ArH), 7.48 (s, 1H, -ArH), 7.51–7.48 (1H, d, *J* = 15.0 Hz, -$CH_\alpha$), 7.65–7.63 (d, 3H, *J* = 10.0 Hz, -ArH), 7.81–7.78 (d, 1H, *J* = 15.0 Hz, -$CH_\beta$). $^{13}$C NMR (125 MHz, $CDCl_3$) δ: 101.81, 101.88, 107.78, 107.79, 108.44, 121.46, 124.69, 128.39, 128.94, 130.42, 144.27, 148.30, 151.71, 188.27. ESI-MS (*m/z*): Calculated- 252.2646, Observed-252.2599.

#### 4.1.2. (2E)-1-(2H-1,3-benzodioxol-5-yl)-3-(4-hydroxyphenyl)prop-2-en-1-one (O2)

Yield: 51%. $^{1}$H NMR (500 MHz, $CDCl_3$)δ: 5.81 (s, 1H, OH), 6.07 (s, 2H, O-$CH_2$-O), 6.91–6.89 (d, 2H, *J* = 10.0 Hz, -ArH), 6.96–6.94 (d, 1H, *J* = 10.0 Hz, -ArH), 7.40–7.36 (1H, d, *J* = 16.0 Hz, -$CH_\alpha$), 7.62–7.60 (d, 2H, *J* = 10.0 Hz, -ArH), 7.64–7.63 (d, 1H, *J* = 10.0 Hz, -ArH), 7.80–7.77 (d, 1H, *J* = 15.0 Hz, -$CH_\beta$). $^{13}$C NMR (125 MHz, $CDCl_3$) δ: 101.80, 101.79, 107.66, 107.77, 108.14, 121.26, 124.62, 128.19, 128.44, 130.44, 144.26, 148.35, 151.51, 188.37. ESI-MS (*m/z*): Calculated- 268.2640, Observed-268.2789.

#### 4.1.3. (2E)-1-(2H-1,3-benzodioxol-5-yl)-3-(4-methoxyphenyl)prop-2-en-1-one (O3)

Yield: 79%. $^{1}$H NMR (500 MHz, $CDCl_3$)δ: 3.85 (s, 3H, $OCH_3$), 6.06 (s, 2H, O-$CH_2$-O), 6.90–6.88 (d, 2H, *J* = 10.0 Hz, -ArH), 6.95–6.93 (d, 1H, *J* = 10.0 Hz, -ArH), 7.39–7.36 (1H, d, *J* = 15.0 Hz, -$CH_\alpha$), 7.53 (s, 1H, -ArH), 7.60–7.58, (d, 2H, *J* = 10.0 Hz, -ArH), 7.65–7.63 (d, 1H, *J* = 10.0 Hz, -ArH), 7.79–7.76 (d, 1H, *J* = 15.0 Hz, -$CH_\beta$). $^{13}$C NMR (125 MHz, $CDCl_3$) δ: 54.41, 101.82, 107.88, 108.41, 114.37, 119.32, 123.45, 124.48, 127.68, 130.09, 130.22, 144.12, 148.22, 151.51, 161.55, 188.31. ESI-MS (*m/z*): Calculated- 282.2906, Observed-

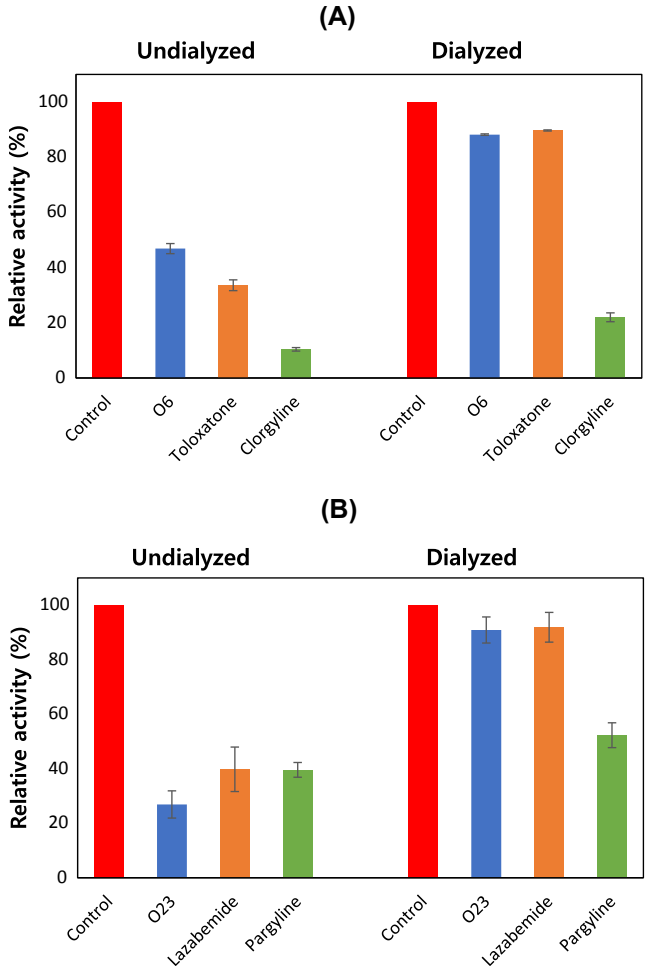


**Fig. 3.** Recoveries of MAO-A and MAO-B inhibitions by O6 (A) and O23 (B), respectively, as determined by dialysis.

282.2879.

*4.1.4. (2E)-1-(2H-1,3-benzodioxol-5-yl)-3-(4-methylphenyl)prop-2-en-1-one (**O4**)*

Yield: 75%. $^{1}$H NMR (500 MHz, $CDCl_3$)δ: 2.39 (s, 3H, $CH_3$), 6.07 (s, 2H, O-$CH_2$-O), 6.91–6.88 (d, 1H, *J* = 10.0 Hz, -ArH), 7.23–7.21 (d, 2H, *J* = 10.0 Hz, -ArH), 7.47–7.42 (1H, d, *J* = 15.0 Hz, -$CH_\alpha$), 7.55–7.53, (d, 2H, *J* = 10.0 Hz, -ArH), 7.64 (s, 1H, -ArH), 7.67–7.65 (d, 1H, *J* = 10.0 Hz, -ArH), 7.80–7.77 (d, 1H, *J* = 15.0 Hz, -$CH_\beta$). $^{13}$C NMR (125 MHz, $CDCl_3$) δ: 21.53, 101.84, 107.89, 108.43, 120.65, 124.60, 127.23, 128.41, 129.68, 132.21, 133.08, 140.94, 144.36, 148.25, 151.61, 188.37. ESI-MS (*m/z*): Calculated- 266.2912, Observed-266.2899.

**Table 2**
Trypan blue dye exclusion *in vitro* cytotoxicity test.

| Drug concentration (μg/mL) | Percentage of cell death (%) | |
|---|---|---|
| | O10 | O23 |
| 200 | 11 | 4 |
| 100 | 5 | – |
| 50 | – | – |
| 20 | – | – |
| 10 | – | – |

**Table 3**
Docking scores and binding free energy values of **O10** and **O23** for MAO-A and MAO-B.

| Code | MAO-A | | MAO-B | |
|---|---|---|---|---|
| | Docking score (kcal/mol) | Binding free energy (kcal/mol) | Docking score (kcal/mol) | Binding free energy (kcal/mol) |
| O10 | −8.598 | −27.13 | −10.092 | −47.70 |
| O23 | −8.593 | −34.16 | −10.220 | −55.48 |

*4.1.5. (2E)-1-(2H-1,3-benzodioxol-5-yl)-3-[4-(dimethylamino)phenyl] prop-2-en-1-one (**O5**)*

Yield: 74%. $^{1}$H NMR (500 MHz, $CDCl_3$)δ: 3.04 (s, 6H, N($CH_3$)$_2$), 6.05 (s, 2H, O-$CH_2$-O), 6.91–6.89 (d, 1H, *J* = 10.0 Hz, -ArH), 6.68–6.66 (d, 2H, *J* = 10.0 Hz, -ArH), 6.89–6.87 (d, 1H, -ArH), 7.31–7.28 (1H, d, *J* = 15.0 Hz, -$CH_\alpha$), 7.55–7.53, (d, 3H, *J* = 10.0 Hz, -ArH), 7.65–7.63 (d, 1H, *J* = 10.0 Hz, -ArH), 7.79–7.76 (d, 1H, *J* = 15.0 Hz, -$CH_\beta$). $^{13}$C NMR (125 MHz, $CDCl_3$) δ: 40.15, 101.71, 107.83, 108.41, 111.79, 112.00, 116.41, 122.70, 124.17, 130.32, 133.74, 142.80, 145.26, 148.07, 151.15, 151.19, 188.43. ESI-MS (*m/z*): Calculated- 295.3324, Observed-295.3298.

*4.1.6. (2E)-1-(2H-1,3-benzodioxol-5-yl)-3-(4-ethylphenyl)prop-2-en-1-one (**O6**)*

Yield: 77%. $^{1}$H NMR (500 MHz, $CDCl_3$)δ: 1.27–1.25 (t, 3H , *J* = 10.0 Hz, $CH_3$), 2.71–2.69 (q, 2H , *J* = 10.0 Hz, $CH_2$), 6.04 (s, 2H, O-$CH_2$-O), 6.90–6.88 (d, 1H, *J* = 10.0 Hz, -ArH), 7.25–7.23 (d, 1H, *J* = 10.0 Hz, -ArH), 7.47–7.43 (1H, d, *J* = 15.0 Hz, -$CH_\alpha$), 7.55–7.53, (d, 3H, *J* = 10.0 Hz, -ArH), 7.57 (s, 1H, -ArH), 7.65–7.63 (d, 1H, *J* = 10.0 Hz, -ArH), 7.80–7.77 (d, 1H, *J* = 15.0 Hz, -$CH_\beta$). $^{13}$C NMR (125 MHz, $CDCl_3$) δ: 15.35, 28.84, 101.84, 107.88, 107.96 108.42, 120.68, 124.59, 128.50, 132.44, 144.37, 147.23, 148.24, 151.60, 188.34, 196.77. ESI-MS (*m/z*): Calculated- 280.3178, Observed-280.3091.

*4.1.7. (2E)-1-(2H-1,3-benzodioxol-5-yl)-3-(4-nitrophenyl)prop-2-en-1-one (**O7**)*

Yield: 80%. $^{1}$H NMR (500 MHz, $CDCl_3$)δ: 6.07 (s, 2H, O-$CH_2$-O), 6.93–6.91 (d, 1H, *J* = 10.0 Hz, -ArH), 7.26–7.24 (d, 2H, *J* = 10.0 Hz, -ArH), 7.62–7.59 (1H, d, *J* = 15.0 Hz, -$CH_\alpha$), 7.68 (s, 1H, -ArH),

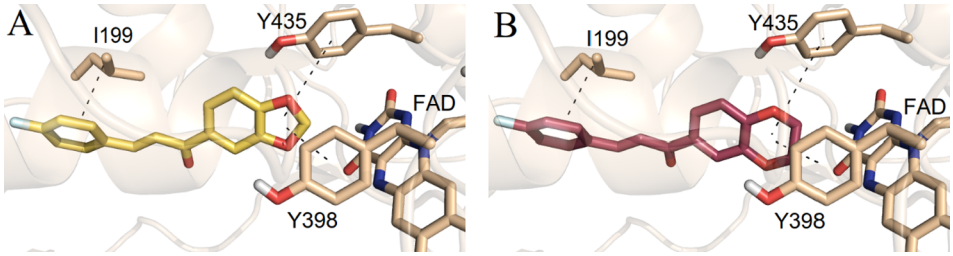


**Fig. 4.** Top-scored docking poses of O10 (A) and O23 (B) in MAO B. Proteins are rendered as cartoons while ligands and important residues are rendered as sticks. For the clarity of description, only polar hydrogen atoms are shown. Black and red lines indicate possible hydrophobic and hydrogen bond interactions.

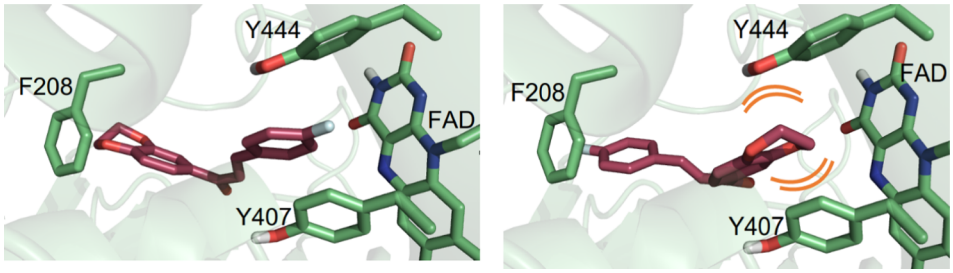


**Fig. 5.** Left-hand and right-hand poses produced the binding energies of −8.593 kcal/mol and −8.061 kcal/mol, respectively, for the docking of O23 with MAO-A. Proteins are rendered as cartoons while ligands and important residues are rendered as sticks. Orange bows indicate steric hindrance.

7.77–7.79, (d, 2H, *J* = 10.0 Hz, -ArH), 7.81–7.78 (d, 1H, *J* = 15.0 Hz, -$CH_\beta$), 8.28–8.26 (d, 2H, *J* = 10.0 Hz, -ArH). $^{13}$C NMR (125 MHz, $CDCl_3$) δ: 101.95, 102.06, 107.95, 108.04, 124.22, 125.05, 125.44, 127.43, 128.50, 132.33, 140.98, 141.17, 152.24, 187.35. ESI-MS (*m/z*): Calculated- 297.2622, Observed-297.2598.

*4.1.8. (2E)-1-(2H-1,3-benzodioxol-5-yl)-3-(4-chlorophenyl)prop-2-en-1-one (**O8**)*

Yield: 73%. $^1$H NMR (500 MHz, $CDCl_3$)δ: 6.06 (s, 2H, O-$CH_2$-O), 6.91–6.89 (d, 1H, *J* = 10.0 Hz, -ArH), 7.40–7.38 (d, 2H, *J* = 10.0 Hz, -ArH), 7.40–7.38 (d, 2H, -ArH), 7.48–7.45 (1H, d, *J* = 15.0 Hz, -$CH_\alpha$), 7.53 (s, 1H, *J* = 10.0 Hz, -ArH),7.58–7.56, (d, 1H, *J* = 10.0 Hz, -ArH), 7.73–7.73 (d, 1H, *J* = 15.0 Hz, -$CH_\beta$). $^{13}$C NMR (125 MHz, $CDCl_3$) δ: 101.92, 107.95, 108.41, 122.08, 124.74, 129.22, 129.53, 132.78, 133.47, 136.28, 142. 76, 151.85, 187.96. ESI-MS (*m/z*): Calculated- 286.7097, Observed-286.6999.

*4.1.9. (2E)-1-(2H-1,3-benzodioxol-5-yl)-3-(4-bromophenyl)prop-2-en-1-one (**O9**)*

Yield: 76%. $^1$H NMR (500 MHz, $CDCl_3$)δ: 6.06 (s, 2H, O-$CH_2$-O), 6.91–6.89 (d, 1H, *J* = 10.0 Hz, -ArH), 7.49–7.46 (1H, d, *J* = 15.0 Hz, -$CH_\alpha$), 7.55–7.50 (d, 5H, -ArH), 7.65–7.63 (d, 1H, *J* = 10.0 Hz, -ArH),7.40–7.38 (d, 2H, *J* = 10.0 Hz, -ArH), 7.40–7.38 (d, 2H, -ArH), 7.73–7.70 (d, 1H, *J* = 15.0 Hz, -$CH_\beta$). $^{13}$C NMR (125 MHz, $CDCl_3$) δ: 101.86, 102.02, 107.93, 108.39, 122.15, 124.63, 129.72, 131.61, 132.75, 133.87, 142.79, 148.35, 151.85, 187.92. ESI-MS (*m/z*): Calculated- 331.1607, Observed-331.1599.

*4.1.10. (2E)-1-(2H-1,3-benzodioxol-5-yl)-3-(4-fluorophenyl)prop-2-en-1-one (**O10**)*

Yield: 76%. $^1$H NMR (500 MHz, $CDCl_3$)δ: 6.03 (s, 2H, O-$CH_2$-O), 6.91–6.89 (d, 1H, *J* = 10.0 Hz, -ArH), 7.11–7.09 (d, 2H, *J* = 10.0 Hz, -ArH), 7.43–7.40 (d, 1H, *J* = 15.0 Hz, -$CH_\alpha$), 7.52 (s, 1H, -ArH), 7.63–7.61 (d, 3H, *J* = 10.0 Hz, -ArH), 7.77–7.74 (d, 1H, *J* = 15.0 Hz, -$CH_\beta$). $^{13}$C NMR (125 MHz, $CDCl_3$) δ: 101.99, 107.97, 108.40, 116.01, 121.35, 124.68, 130.23, 142.94, 148.33, 151.80, 162.97, 164.97, 188.03, 196.45. ESI-MS (*m/z*): Calculated- 270.2551, Observed-270.2489.

*4.1.11. (2E)-1-(2H-1,3-benzodioxol-5-yl)-3-(3-fluorophenyl)prop-2-en-1-one (**O11**)*

Yield: 74%. $^1$H NMR (500 MHz, $CDCl_3$)δ: 6.03 (s, 2H, O-$CH_2$-O), 6.91–6.89 (d, 1H, *J* = 10.0 Hz, -ArH), 7.11–7.09 (d, 2H, *J* = 10.0 Hz, -ArH), 7.40–7.39 (d, 3H, , *J* = 5.0 Hz, -ArH), 7.49–7.46 (d, 1H, *J* = 15.0 Hz, -$CH_\alpha$), 7.53 (s, 1H, -ArH), 7.66–7.64 (d, 1H, *J* = 10.0 Hz, -ArH), 7.75–7.72 (d, 1H, *J* = 15.0 Hz, -$CH_\beta$). $^{13}$C NMR (125 MHz, $CDCl_3$) δ: 101.85, 101.93, 107.95, 122.82, 124.47, 124.81, 130.44, 130.51, 142.71, 142.73, 151.89, 162.04, 164.00, 187.88, 196.22. ESI-MS (*m/z*): Calculated- 270.2551, Observed-270.00.

*4.1.12. (2E)-1-(2H-1,3-benzodioxol-5-yl)-3-(2-fluorophenyl)prop-2-en-1-one (**O12**)*

Yield: 68%. $^1$H NMR (500 MHz, $CDCl_3$)δ: 6.06 (s, 2H, O-$CH_2$-O), 6.91–6.89 (d, 1H, *J* = 10.0 Hz, -ArH), 7.15–7.13 (d, 1H, *J* = 10.0 Hz, -ArH), 7.54 (s, 1H, -ArH), 7.62–7.59 (d, 1H, *J* = 15.0 Hz, -$CH_\alpha$), 7.66–7.64 (d, 4H, *J* = 10.0 Hz, -ArH), 7.89–7.86 (d, 1H, *J* = 15.0 Hz, -$CH_\beta$). $^{13}$C NMR (125 MHz, $CDCl_3$) δ: 101.81, 101.90, 107.93, 124.46, 124.85, 129.82, 131.65, 137.01, 148.32, 151.81, 160.69, 161.95, 162.71, 188.24, 196.47. ESI-MS (*m/z*): Calculated- 270.2551, Observed-270.2488.

*4.1.13. (2E)-1-(2H-1,3-benzodioxol-5-yl)-3-[4-(trifluoromethyl)phenyl] prop-2-en-1-one (**O13**)*

Yield: 69%. $^1$H NMR (500 MHz, $CDCl_3$)δ: 6.08 (s, 2H, O-$CH_2$-O), 6.91–6.89 (d, 1H, *J* = 10.0 Hz, -ArH), 7.40–7.37 (d, 1H, *J* = 15.0 Hz, -$CH_\alpha$), 7.49 (s, 1H, -ArH), 7.52–7.50 (d, 2H, *J* = 10.0 Hz, -ArH), 763–7.61 (d, 2H, *J* = 10.0 Hz, -ArH), 7.74–7.72 (d, 1H, *J* = 10.0 Hz, -ArH), 7.83–7.81 (d, 4H, *J* = 10.0 Hz, -ArH), 8.12–8.09 (d, 1H, *J* = 15.0 Hz, -$CH_\beta$). ESI-MS (*m/z*): $^{13}$C NMR (125 MHz, $CDCl_3$) δ: 101.95, 107.51, 108.51, 125.06, 126.23, 126.31, 127.92, 129.57, 132.07, 132.42, 134.42, 139.58, 151.96, 188.03. Calculated- 320.2626, Observed-320.2599.

*4.1.14. (2E)-1-(2,3-dihydro-1,4-benzodioxin-6-yl)-3-phenylprop-2-en-1-one (**O14**)*

Yield: 72%. $^1$H NMR (500 MHz, $CDCl_3$)δ: 4.31–4.29 (t, 4H, *J* = 10.0 Hz, O-$CH_2$-$CH_2$-O), 6.95–6.93 (d, 1H, *J* = 10.0 Hz, -ArH), 7.42–7.40, (d, 3H, *J* = 10.0 Hz, -ArH), 7.52–7.49 (1H, d, *J* = 15.0 Hz, -$CH_\alpha$),7.63 (s, 1H, -ArH), 7.65–7.63 (d, 3H, *J* = 10.0 Hz, -ArH), 7.81–7.78 (d, 1H, *J* = 15.0 Hz, -$CH_\beta$). $^{13}$C NMR (125 MHz, $CDCl_3$) δ: 64.70, 117.17, 118.05, 121.70, 122.67, 127.97, 128.07, 128.93, 130.37, 131.92, 135.01, 143.43, 144.11, 147.94, 188.55. ESI-MS (*m/z*): Calculated- 266.2912, Observed-266.2921.

*4.1.15. (2E)-1-(2,3-dihydro-1,4-benzodioxin-6-yl)-3-(4-hydroxyphenyl) prop-2-en-1-one (**O15**)*

Yield: 47%. $^1$H NMR (500 MHz, $CDCl_3$)δ: 4.30–4.28 (t, 4H, *J* = 10.0 Hz, O-$CH_2$-$CH_2$-O), 6.94–6.92 (d, 1H, *J* = 10.0 Hz, -ArH), 7.44–7.42, (d, 3H, *J* = 10.0 Hz, -ArH), 7.51–7.48 (1H, d, *J* = 15.0 Hz, -$CH_\alpha$), 7.65–7.63 (d, 3H, *J* = 10.0 Hz, -ArH), 7.80–7.77 (d, 1H, *J* = 15.0 Hz, -$CH_\beta$). $^{13}$C NMR (125 MHz, $CDCl_3$) δ: 64.99, 117.15, 118.35, 121.71, 122.17, 127.53, 128.17, 128.53, 130.35, 131.62, 135.80, 143.44, 144.71, 147.44, 188.35. ESI-MS (*m/z*): Calculated- 282.2906, Observed-282.2899.

*4.1.16. (2E)-1-(2,3-dihydro-1,4-benzodioxin-6-yl)-3-(4-methoxyphenyl) prop-2-en-1-one (**O16**)*

Yield: 82%. $^1$H NMR (500 MHz, $CDCl_3$)δ: 3.85 (s, 3H, $OCH_3$), 4.32–4.30 (t, 4H, *J* = 10.0 Hz, O-$CH_2$-$CH_2$-O), 6.94–6.92 (d, 2H, *J* = 10.0 Hz, -ArH), 6.95 (s, 1H, -ArH), 7.40–7.37 (1H, d, *J* = 15.0 Hz, -$CH_\alpha$), 7.60–7.58, (d, 4H, *J* = 10.0 Hz, -ArH), 7.78–7.75 (d, 1H, *J* = 15.0 Hz, -$CH_\beta$). $^{13}$C NMR (125 MHz, $CDCl_3$) δ: 54.41, 64.69,

114.35, 117.22, 119.37, 122.54, 123.45, 127.73, 130.13, 132.20, 143.37, 143.96, 147.74, 161.51, 188.59. ESI-MS (*m/z*): Calculated-296.3172, Observed-296.3099.

*4.1.17. (2E)-1-(2,3-dihydro-1,4-benzodioxin-6-yl)-3-(4-methylphenyl) prop-2-en-1-one* ***(O17)***

Yield: 81%. $^1$H NMR (500 MHz, $CDCl_3$)δ: 2.39 (s, 3H, $OCH_3$), 4.33–4.31 (t, 4H, *J* = 10.0 Hz, O-$CH_2$-$CH_2$-O), 6.96–6.94 (d, 2H, *J* = 10.0 Hz, -ArH), 7.23–7.21 (d, 2H, *J* = 10.0 Hz, -ArH), 7.48–7.45 (1H, d, *J* = 15.0 Hz, -$CH_\alpha$), 7.54–7.52, (d, 1H, *J* = 10.0 Hz, -ArH), 7.60–7.58, (d, 2H, *J* = 10.0 Hz, -ArH), 7.79–7.76 (d, 1H, *J* = 15.0 Hz, -$CH_\beta$). $^{13}$C NMR (125 MHz, $CDCl_3$) δ: 21.53, 64.70, 117.26, 118.26, 120.69, 122.62, 124.56, 128.41, 129.66, 132.27, 140.88, 143.18, 143.40, 144.21, 147.83, 188.65. ESI-MS (*m/z*): Calculated- 280.3178, Observed-280.3099.

*4.1.18. (2E)-1-(2,3-dihydro-1,4-benzodioxin-6-yl)-3-[4-(dimethylamino) phenyl]prop-2-en-1-one* ***(O18)***

Yield: 80%. $^1$H NMR (500 MHz, $CDCl_3$)δ: 3.04 (s, 6H, $N(CH_3)_2$), 4.32–4.30 (t, 4H, *J* = 10.0 Hz, O-$CH_2$-$CH_2$-O), 6.95–6.93 (d, 1H, *J* = 10.0 Hz, -ArH), 7.62–7.60 (d, *J* = 10.0 Hz, 6H, ArH), 7.33–7.30 (1H, d, *J* = 15.0 Hz, -$CH_\alpha$), 7.79–7.76 (d, 1H, *J* = 15.0 Hz, -$CH_\beta$). $^{13}$C NMR (125 MHz, $CDCl_3$) δ: 40.16, 64.67, 111.25, 116.49, 117.84, 120.31, 122.40, 130.30, 132.76, 141.45, 145.09, 151.89, 188.70. ESI-MS (*m/z*): Calculated- 309.3590, Observed-309.3498.

*4.1.19. (2E)-1-(2,3-dihydro-1,4-benzodioxin-6-yl)-3-(4-ethylphenyl)prop-2-en-1-one* ***(O19)***

Yield:75%. $^1$H NMR (500 MHz, $CDCl_3$)δ: 1.28–1.26 (t, 3H , *J* = 10.0 Hz, $CH_3$), 2.69–2.67 (q, 2H , *J* = 10.0 Hz, $CH_2$), 4.30–4.28 (t, 4H, *J* = 10.0 Hz, O-$CH_2$-$CH_2$-O), 6.92–6.90 (d, 1H, *J* = 10.0 Hz, -ArH), 7.28–7.26 (d, 1H, *J* = 10.0 Hz, -ArH), 7.45–7.42 (1H, d, *J* = 15.0 Hz, -$CH_\alpha$), 7.57–7.55, (d, 3H, *J* = 10.0 Hz, -ArH), 7.58 (s, 1H, -ArH), 7.65–7.63 (d, 1H, *J* = 10.0 Hz, -ArH), 7.81–7.78 (d, 1H, *J* = 15.0 Hz, -$CH_\beta$).$^{13}$C NMR (125 MHz, $CDCl_3$) δ: 15.33, 28.84, 66.65, 101.14, 107.08, 107.926 108.44, 120.08, 124.53, 128.53, 132.44, 144.17, 147.53, 148.26, 151.62, 188.44, 196.17. ESI-MS (*m/z*): Calculated-294.3444, Observed-294.3399.

*4.1.20. (2E)-1-(2,3-dihydro-1,4-benzodioxin-6-yl)-3-(4-nitrophenyl)prop-2-en-1-one* ***(O20)***

Yield:72%. $^1$H NMR (500 MHz, $CDCl_3$)δ: 4.31–4.29 (t, 4H, *J* = 10.0 Hz, O-$CH_2$-$CH_2$-O), 7.00–6.90 (d, 1H, *J* = 10.0 Hz, -ArH), 7.623–7.60 (1H, d, *J* = 15.0 Hz, -$CH_\alpha$), 7.78–7.78 (d, 4H, *J* = 10.0 Hz, -ArH), 7.81–7.78 (d, 1H, *J* = 15.0 Hz, -$CH_\beta$), 8.28–8.26 (d, 2H, *J* = 10.0 Hz, -ArH). $^{13}$C NMR (125 MHz, $CDCl_3$) δ: 64.66, 117.17, 117.49, 118.13, 122.47, 122.84, 124.19, 125.46, 128.86, 131.12, 140.82, 141.23, 143.58, 144.71, 148.45, 187.65. ESI-MS (*m/z*): Calculated- 311.2888, Observed-311.2798.

*4.1.21. (2E)-3-(4-chlorophenyl)-1-(2,3-dihydro-1,4-benzodioxin-6-yl) prop-2-en-1-one* ***(O21)***

Yield: 81%. $^1$H NMR (500 MHz, $CDCl_3$) δ: 4.34–4.32 (t, 4H, *J* = 10.0 Hz, O-$CH_2$-$CH_2$-O), 6.96–6.94(1H, d, *J* = 10.0 Hz, -ArH), 7.39–7.37 (2H, d, *J* = 10.0 Hz, -ArH), 7.48–7.45 (1H, d, *J* = 15.0 Hz, -$CH_\alpha$), 7.59–7.57 (4H, d, *J* = 10.0 Hz, -ArH), 7.74–7.71 (d, 1H, *J* = 15.0 Hz, -$CH_\beta$). $^{13}$C NMR (125 MHz, $CDCl_3$) δ: 64.12, 117.17, 117.81, 118.03, 122.01, 122.68, 129.218, 129.52, 132.72, 133.50, 136.19, 142.56, 143.46, 148.06, 188.21, 196.70. ESI-MS (*m/z*): Calculated- 300.7363, Observed-300.00.

*4.1.22. (2E)-3-(4-bromophenyl)-1-(2,3-dihydro-1,4-benzodioxin-6-yl) prop-2-en-1-one* ***(O22)***

Yield: 63%. $^1$H NMR (500 MHz, $CDCl_3$) δ: 4.35–4.33 (t, 4H, *J* = 10.0 Hz, O-$CH_2$-$CH_2$-O), 6.97–6.95(1H, d, *J* = 10.0 Hz, -ArH), 7.48–7.46 (2H, d, *J* = 10.0 Hz, -ArH), 7.53–7.50 (1H, d, *J* = 15.0 Hz, -$CH_\alpha$), 7.59–7.57 (4H, d, *J* = 10.0 Hz, -ArH), 7.73–7.70 (d, 1H, *J* = 15.0 Hz, -$CH_\beta$). $^{13}$C NMR (125 MHz, $CDCl_3$) δ: 64.13, 117.35, 118.04, 122.20, 122.69, 124.58, 129.73, 130.86, 131.75, 132.15, 133.94, 142.65, 143.47, 148.07, 188.23. ESI-MS (*m/z*): Calculated-345.1873, Observed-345.1799.

*4.1.23. (2E)-1-(2,3-dihydro-1,4-benzodioxin-6-yl)-3-(4-fluorophenyl) prop-2-en-1-one* ***(O23)***

Yield: 72%. $^1$H NMR (500 MHz, $CDCl_3$) δ: 4.34–4.32 (t, 4H, *J* = 10.0 Hz, O-$CH_2$-$CH_2$-O), 6.96–6.94 (1H, d, *J* = 10.0 Hz, -ArH), 6.97–6.95(1H, d, *J* = 10.0 Hz, -ArH), 7.12–7.10 (d, 1H, *J* = 15.0 Hz, -$CH_\beta$), 7.60–7.58 (4H, d, *J* = 10.0 Hz, -ArH), 7.74–7.71 (d, 1H, *J* = 15.0 Hz, -$CH_\beta$). $^{13}$C NMR (125 MHz, $CDCl_3$) δ: 64.14, 116.00, 117.33, 118.03, 121.42, 122.66, 130.22, 131.84, 142.80, 143.46, 148.002, 162.95, 164.95, 188.34. ESI-MS (*m/z*): Calculated- 284.2817, Observed-284.2793.

*4.1.24. (2E)-1-(2,3-dihydro-1,4-benzodioxin-6-yl)-3-(3-fluorophenyl) prop-2-en-1-one* ***(O24)***

Yield: 71%. $^1$H NMR (500 MHz, $CDCl_3$)δ: : 4.32–4.30 (t, 4H, *J* = 10.0 Hz, O-$CH_2$-$CH_2$-O), 6.03 (s, 2H, O-$CH_2$-O), 6.97–6.95 (d, 1H, *J* = 10.0 Hz, -ArH), 7.10–7.08 (d, 1H, *J* = 10.0 Hz, -ArH), 7.39–7.37 (d, 3H, *J* = 10.0 Hz, -ArH), 7.50–7.47 (d, 1H, *J* = 15.0 Hz, -$CH_\alpha$), 7.60–7.58 (d, 2H, *J* = 10.0 Hz, -ArH), 7.75–7.72 (d, 1H, *J* = 15.0 Hz, -$CH_\beta$). $^{13}$C NMR (125 MHz, $CDCl_3$) δ: 64.72, 114.31, 117.36, 118.06, 122.87, 124.87, 130.42, 139.49, 137.26, 142.56, 143.49, 148.12, 162.04, 164.00, 188.19, 196.61. ESI-MS (*m/z*): Calculated- 284.2817, Observed-284.2787.

*4.1.25. (2E)-1-(2,3-dihydro-1,4-benzodioxin-6-yl)-3-(2-fluorophenyl) prop-2-en-1-one* ***(O25)***

Yield: 65%. $^1$H NMR (500 MHz, $CDCl_3$)δ: 4.35–4.35 (t, 4H, *J* = 10.0 Hz, O-$CH_2$-$CH_2$-O), 6.97–6.95 (d, 3H, *J* = 10.0 Hz, -ArH), 7.38–7.35 (d, 1H, *J* = 15.0 Hz, -$CH_\alpha$), 7.63–7.61 (d, 5H, *J* = 10.0 Hz, -ArH), 7.89–7.86 (d, 1H, *J* = 15.0 Hz, -$CH_\beta$). $^{13}$C NMR (125 MHz, $CDCl_3$) δ: 64.74, 117.43, 118.12, 122.78, 123.92, 125.86, 128.89, 131.52, 138.42, 142.04, 143.52, 188.05. ESI-MS (*m/z*): Calculated-284.2817, Observed-284.2794.

*4.1.26. (2E)-1-(2,3-dihydro-1,4-benzodioxin-6-yl)-3-[4-(trifluoromethyl) phenyl]prop-2-en-1-one* ***(O26)***

Yield: 67%. $^1$H NMR (500 MHz, $CDCl_3$)δ: 4.35–4.32 (t, 4H, *J* = 10.0 Hz, O-$CH_2$-$CH_2$-O), 4.35–4.35 (t, 4H, *J* = 10.0 Hz, O-$CH_2$-$CH_2$-O), 6.98–6.96 (d, 1H, *J* = 10.0 Hz, -ArH), 7.58–7.55 (d, 1H, *J* = 15.0 Hz, -$CH_\alpha$), 7.61–7.59 (d, 2H, *J* = 10.0 Hz, -ArH), 7.44–7.42 (d, 4H, *J* = 10.0 Hz, -ArH), 7.80–7.77 (d, 1H, *J* = 15.0 Hz, -$CH_\beta$). $^{13}$C NMR (125 MHz, $CDCl_3$) δ: 64.78, 117.13, 118.22, 122.08, 123.12, 125.83, 128.39, 131.62, 138.62, 142.44, 143.42, 188.35. ESI-MS (*m/z*): Calculated- 334.2892, Observed-334.2799.

### *4.2. Enzyme assays*

#### *4.2.1. Assays of MAO-A and MAO-B*

MAO activities were assayed using recombinant human MAO-A and MAO-B in the presence of 0.06 mM kynuramine (1.7 × $K_m$) or 0.3 mM benzylamine (2.1 × $K_m$) as substrates, respectively, as described previously [55]. $K_m$ values of these substrates were 0.036 mM and 0.14 mM, respectively. Enzymes and chemicals were purchased from Sigma-Aldrich (St. Louis, MO, USA).

#### *4.2.2. Analysis of enzyme inhibition and kinetics*

The inhibitory activities of the 26 compounds against MAO-A and MAO-B were first examined at a concentration of 10 μM, and inhibitory potencies were then determined using $IC_{50}$ values. Time-dependent inhibitions, reversibilities, and kinetic studies were performed on the most potent inhibitors, i.e., **O6** for MAO-A and **O23** for MAO-B, as

previously described [56]. Kinetic experiments were carried out at five substrate and three inhibitor concentrations.

#### 4.2.3. Analysis of inhibitor reversibilities

Reversibilities of compounds **O6** and **O23** were analyzed using a dialysis method after preincubation with MAO-A and MAO-B, respectively, for 30 min, as previously described [57]. The concentrations used were; 0.06 μM for **O6**, 0.0040 μM for **O23**, 2.0 μM for toloxatone (a reversible MAO-A reference inhibitor), 0.014 μM for clorgyline (an irreversible MAO-A reference inhibitor), 0.080 μM for lazabemide (a reversible MAO-B reference inhibitor), and 0.04 μM for pargyline (an irreversible MAO-B reference inhibitor). The relative activities of undialyzed ($A_U$) and dialyzed ($A_D$) samples were compared for determination of reversibility patterns.

### 4.3. Computational studies

#### 4.3.1. Docking methodology

Starting with the fetching from the Protein Data Bank [52,53] of the 3D structures of MAO-A (PDB ID: 2Z5X) and MAO-B (PDB ID: 2V5Z), a pre-treatment of the enzymes was carried out by means of protein preparation module available from the Schrödinger suite [58]: the latter exploits an optimization of a protein structure by adjusting the imprecisions that may occur within a X-ray crystal structure; in doing that, 9 water molecules within MAO-A and 8 water molecules within MAO-B were preserved and not eliminated. The prepared proteins were subjected to docking simulations carried out by using the QM polarized ligand docking available from Schrödinger Suite; such protocol allows a certain conformational flexibility for ligand to be docked while rigidity of the protein structures is retained [59]. The ligand center of mass of the X-ray cognate ligand of both PDB structures was taken as reference for the cubic grid center.

The QM-polarized ligand docking protocol is arranged in three steps, that are: (a) a standard precision (SP) initial docking using Glide; (b) the calculation of QM partial charges of the docked ligand based on the field generated by the receptor; (c) a standard precision (SP) redocking phase upon each ligand pose considering computed QM based charges.

During the analysis of docked poses, steric hindrance between ligands and protein residues was also evaluated according to the following computation of bad contacts:

$$C = \frac{D_{12}}{(R_1 + R_2)}$$

where $D_{12}$ is the distance between atoms 1 and 2, and $R_1$ and $R_2$ are the van der Waals radii of atoms 1 and 2. A range of C values between 0.75 and 0.89 flags a contact between the ligand and the receptor as “bad” [60].

#### 4.3.2. MM-GBSA calculations

In order to estimate ligand-binding affinities, a Molecular Mechanics/Generalized Born Surface Area (MM-GBSA) method was added to the workflow for the calculation of the binding free energies (ΔG) between protein and ligands [61]. Such method is implemented in Prime available in the Schrodinger software 2018-2. Provided that $\Delta E_{MM}$ is the term referred to the minimized energy of the ligand-protein complex, $\Delta G_{solv}$ is the term referred to the solvation energy and $\Delta G_{SA}$ is the term referred to the surface area energy, the binding free energies (ΔG) of compounds with respect to MAO-A and MAO-B were calculated as follows:

$$\Delta G_{bind} = \Delta E_{MM} + \Delta G_{solv} + \Delta G_{SA}$$

Obtained docking poses were minimized using Prime.

#### 4.3.3. ADME-Tox in silico prediction

A panel of pharmaceutically relevant properties (to name a few, the octanol/water and water/gas log Ps, log S, log BB, overall CNS activity, Caco-2 and MDCK cell permeabilities, log Khsa for human serum albumin binding, and log $IC_{50}$ for HERG K+-channel blockage) were calculated by using QiKProp Base a quick, accurate, easy-to-use absorption, distribution, metabolism, and excretion (ADME) [54].

## Declaration of Competing Interest

No conflict of interest declared.

## Acknowledgement

This research was supported by a grant from the Basic Science Research Program of the Korean National Research Foundation (NRF) funded by the Korean Ministry of Education (#2017R1D1A3B03028559), Republic of Korea (to H. Kim).

## Appendix A. Supplementary material

Supplementary data to this article can be found online at https://doi.org/10.1016/j.bioorg.2019.103335.

## References

[1] K.F. Tipton, 90 years of monoamine oxidase: some progress and some confusion, J. Neural Transm. 125 (2018) 1519–1551.
[2] T.P. Singer, R.R. Ramsay, Monoamine oxidases: old friends hold many surprises, FASEB J. 9 (1995) 605–610.
[3] L.G. Iacovino, F. Magnani, C. Binda, The structure of monoamine oxidases: past, present, and future, J. Neural Transm. 125 (2018) 1567–1579.
[4] B. Mathew, G.E. Mathew, J. Suresh, G. Ucar, R. Sasidharan, J.K. Vilapurathu, S. Anbazhagan, V. Jayaprakash, Monoamine oxidase inhibitors: perspective design for the treatment of depression and neurological disorders, Curr. Enzyme Inhib. 12 (2016) 115–122.
[5] S. Carradori, D. Secci, J.P. Petzer, MAO inhibitors and their wider applications: a patent review, Expert Opin. Ther. Pat. 28 (2018) 211–226.
[6] M.B. Youdim, Y.S. Bakhle, Monoamine oxidase: isoforms and inhibitors in Parkinsońs disease and depressive illness. Br J Pharm. 147 (2006) S287–S29.
[7] R.R. Ramsay, Inhibitor design for monoamine oxidases, Curr. Pharm. Des. 19 (2013) 2529–2539.
[8] S. Carradori, R. Silvestri, New frontiers in selective human MAO-B inhibitors, J. Med. Chem. 58 (2015) 6717–6732.
[9] C. Binda, F. Hubalek, M. Li, N. Castagnoli, D.E. Edmondson, A. Mattevi, Structure of the human mitochondrial monoamine oxidase B: new chemical implications for neuroprotectant drug design, Neurology 67 (Issue 7, Supplement 2) (2006) S5–S7, https://doi.org/10.1212/WNL.67.7_suppl_2.S5.
[10] B. Mathew, D.G.T. Parambi, G.E. Mathew, M.S. Uddin, S.T. Inasu, H. Kim, A. Marathakam, M.K. Unnikrishnan, S. Carradori, Emerging therapeutic potentials of dual-acting MAO and AChE inhibitors in Alzheimer's and Parkinson's diseases, Arch. Pharm. Chem. Life Sci. (2019) e1900177.
[11] M. Catto, O. Nicolotti, F. Leonetti, A. Carotti, A.D. Favia, R. Soto-Otero, E. Méndez-Álvarez, A. Carotti, A. Structural insights into monoamine oxidase inhibitory potency and selectivity of 7-substituted coumarins from ligand- and target-based approaches. J. Med. Chem. 49 (2006) 4912–4925.
[12] L. Pisani, R. Farina, M. Catto, R. Iacobazzi, O. Nicolotti, S. Cellamare, G.F. Mangiatordi, N. Denora, R. Soto-Otero, L. Siragusa, C. Altomare, A. Carotti, Exploring basic tail modifications of coumarin-based dual acetylcholinesterase-monoamine oxidase B inhibitors: identification of water-soluble, brain-permeant neuroprotective multitarget agents, J. Med. Chem. 59 (2016) 6791–6806.
[13] G.F. Mangiatordi, D. Alberga, L. Pisani, D. Gadaleta, D. Trisciuzzi, R. Farina, A. Carotti, G. Lattanzi, M. Catto, O. Nicolotti, A rational approach to elucidate human monoamine oxidase molecular selectivity of coumarin-based inhibitors, Eur. J. Pharm. Sci. 101 (2017) 90–99.
[14] L. Pisani, G. Muncipinto, T.F. Miscioscia, O. Nicolotti, F. Leonetti, M. Catto, C. Caccia, P. Salvati, R. Soto-Otero, E. Mendez-Alvarez, C. Passeleu, A. Carotti, Discovery of a novel class of potent coumarin monoamine oxidase B inhibitors: Development and biopharmacological profiling of 7-[(3-chlorobenzyl) oxy]-4-[(methylamino)methyl]-2H-chromen-2-one methanesulfonate (NW-1772) as a highly potent, selective, reversible, and orally active monoamine oxidase B inhibitor, J. Med. Chem. 52 (2009) 6685–6706.
[15] L. Pisani, M. Catto, O. Nicolotti, G. Grossi, M. Di Braccio, R. Soto-Otero, E. Mendez-Alvarez, A. Stefanachi, D. Gadaleta, A. Carotti, Fine molecular tuning at position 4 of 2H-chromen-2-one derivatives in the search of potent and selective monoamine oxidase B inhibitors, Eur. J. Med. Chem. 70 (2013) 723–739.
[16] L. Pisani, R. Farina, O. Nicolotti, D. Gadaleta, R. Soto-Otero, M. Catto, M. Di Braccio, E. Mendez-Alvarez, A. Carotti, In silico design of novel 2H-chromen-2-one derivatives as potent and selective MAO-B inhibitors, Eur. J. Med. Chem. 89 (2014) 98–105.

[17] R. Farina, L. Pisani, M. Catto, O. Nicolotti, D. Gadaleta, N. Denora, R. Soto-Otero, E. Méndez-Álvarez, C. Passos, G. Muncipinto, C.D. Altomare, A. Nurisso, P.A. Carrupt, A. Carotti, Structure-based design and optimization of multitarget-directed 2H-chromen-2-one derivatives as potent inhibitors of monoamine oxidase B and cholinesterases, J. Med. Chem. 58 (2015) 5561–5578.

[18] L. Pisani, R. Farina, R. Soto-Otero, N. Denora, G.F. Mangiatordi, O. Nicolotti, E. Mendez-Álvarez, C.D. Altomare, M. Catto, A. Carotti, Searching for multi-targeting Neurotherapeutics against Alzheimer's: discovery of potent AChE-MAO B inhibitors through the decoration of 2H-Chromen-2-one structural motif, Molecules 21 (2016) 3–15.

[19] B. Mathew, Unraveling the structural requirements of chalcone chemistry towards monoamine oxidase inhibition, Cent. Nerv. Syst. Agents Med. Chem. 19 (2019) 6–7.

[20] B. Mathew, A. Haridas, J. Suresh, G.E. Mathew, G. Ucar, V. Jayaprakash, Monoamine oxidase inhibitory actions of chalcones. a mini review, Cent. Nerv. Syst. Agents Med. Chem. 16 (2016) 120–136.

[21] F. Chimenti, R. Fioravanti, A. Bolasco, P. Chimenti, D. Secci, F. Rossi, M. Yanez, F. Orallo, F. Ortuso, S. Alcaro, Chalcones: a valid scaffold for monoamine oxidases inhibitors, J. Med. Chem. 52 (2009) 2818–2824.

[22] B. Mathew, G.E. Mathew, G. Ucar, M. Joy, E.K. Nafna, K.K. Lohidakshan, J. Suresh, Monoamine oxidase inhibitory activity of methoxy-substituted chalcones, Int. J. Bio. Macromol. 104 (2017) 1321–1329.

[23] B. Mathew, G.E. Mathew, G. Uçar, I. Baysal, J. Suresh, J.K. Vilapurathu, A. Prakasan, J.K. Suresh, A. Thomas. Development of fluorinated methoxylated chalcones as selective monoamine oxidase-B inhibitors: synthesis, biochemistry and molecular docking studies. Bioorg. Chem. 62 (2015) 22–29.

[24] A. Hammuda, R. Shalaby, S. Rovida, D.E. Edmondson, C. Binda, A. Khali, Design and synthesis of novel chalcones as potent selective monoamine oxidase-B, Eur. J. Med. Chem. 114 (2016) 162–169.

[25] B. Mathew, G.E. Mathew, G. Ucar, I. Baysal, J. Suresh, S. Mathew, Potent and selective monoamine oxidase-b inhibitory activity: fluoro- vs trifluoromethyl-4-hydroxylated chalcone derivatives, Chem. Biodivers. 13 (2016) 1046–1052.

[26] B. Mathew, G. Ucar, G.E. Mathew, S. Mathew, P.K. Purapurath, F. Moolayil, S. Mohan, S.V. Gupta, Monoamine oxidase inhibitory activity: methyl- versus chloro-chalcone derivatives, ChemMedChem 11 (2016) 2649–2655.

[27] B. Lakshminarayan, S.C. Baek, N. Kannappan, G.F. Mangiatordi, O. Nicolotti, T. Subburaju, H. Kim, B. Mathew, Ethoxylated head of chalcones as a new class of Multi-targeted MAO inhibitors, ChemistrySelect 4 (2019) 6614–6619.

[28] C. Zhuang, W. Zhang, C. Sheng, W. Zhang, C. Xing, Z. Miao, Chalcone. A privileged structure in medicinal chemistry, Chem. Rev. 117 (2017) 7762–7810.

[29] B. Mathew, D.G.T. Parambi, M.S. Uddin, J. Suresh, G.E. Mathew, M. Joy, A. Marathakam, S.V. Gupta, Perspective design of chalcones for the management of CNS disorders: a mini-review, CNS Neurol. Disord. Drug Targets 18 (2019) 432–445.

[30] J.A.H. Schwöbel, D. Wondrousch, Y.K. Koleva, J.C. Madden, M.T.D. Cronin, G. Schüürmann, Prediction of michael-type acceptor reactivity toward glutathione, Chem. Res. Toxicol. 23 (2010) 1576–1585.

[31] M.D. Kar, V. Asati, S.K. Bharti, An updated patent review of therapeutic applications of chalcone derivatives (2014-present), Expert. Opin. Ther. Pat. 29 (2019) 385–406.

[32] A. Gaulton, A. Hersey, M. Nowotka, A.P. Bento, J. Chambers, D. Mendez, P. Mutowo, F. Atkinson, L.J. Bellis , E. Cibrián-Uhalte. et al. The ChEMBL database in 2017. Nucleic Acids Res. 45 (2017) D945–D954.

[33] M. Montaruli, D. Alberga, F. Ciriaco, D. Trisciuzzi, A.R. Tondo, G.F. Mangiatordi, O. Nicolotti, Accelerating drug discovery by early protein drug target prediction based on multi-fingerprint similarity search, Molecules 24 (2019) 2233.

[34] O. Nicolotti, T.F. Miscioscia, F. Leonetti, G. Muncipinto, A. Carotti, Screening of matrix metalloproteinases available from the protein data bank: Insights into biological functions, domain organization, and zinc binding groups, J. Chem. Inform. Model. 47 (2007) 2439–2448.

[35] D. Alberga, D. Trisciuzzi, M. Montaruli, F. Leonetti, G.F. Mangiatordi, O. Nicolotti, A new approach for drug target and bioactivity prediction: the Multi-fingerprint Similarity Search aLgorithm (MuSSeL), J. Chem. Inform. Model 59 (2019) 586–596.

[36] B. Mathew, J. Suresh, S. Anbazhagan, J. Paulra, G.K. Krishnan, Heteroaryl chalcones: mini review about their therapeutic voyage, Bio. Med. Prev. Nut. 4 (2014) 451–458.

[37] S.J. Robinson, J.P. Petzer, A. Petzer, J.J. Bergh, A.C.U. Lourens, Selected furanochalcones as inhibitors of monoamine oxidase, Bioorg. Med. Chem. Lett. 23 (2013) 4985–4989.

[38] C. Minders, J.P. Petzer, A. Petzer, A.C.U. Lourens ACU. Monoamine oxidase inhibitory activities of heterocyclic chalcones. Bioorg. Med. Chem. Lett. 25 (2015) 5270–5276.

[39] B. Mathew, G. Uçar, S. Yabanoğlu-Çiftçi, I. Baysal, J. Suresh, G.E. Mathew, J.K. Vilapurathu, A.M. Nadeena, P. Nabeela, V. Lakshmi, Development of fluorinated thienylchalcones as monoamine oxidase-b inhibitors: design, synthesis, biological evaluation and molecular docking studies, Lett. Org. Chem. 12 (2015) 605–613.

[40] B. Mathew, A. Haridas, G. Uçar, I. Baysal, A.A. Adeniyi, M.E.S. Soliman, Exploration of chlorinated thienyl chalcones: a new class of Monoamine oxidase-B inhibitors, Int. J. Biol. Macromol. 91 (2016) 680–695.

[41] B. Mathew, A. Haridas, G. Uçar, I. Baysal, M. Joy, G.E. Mathew, B. Lakshmanan, V. Jayaprakash, Synthesis, biochemistry, and computational studies of brominated thienyl chalcones: a new class of reversible MAO-B inhibitors, ChemMedChem 11 (2016) 1161–1171.

[42] R. Sasidharan, S.L. Manju, G. Ucar, I. Baysal, B. Mathew, Identification of indole based chalcones: discovery of potent, selective and reversible class of MAO-B inhibitors, Arch. Pharm. Chem. Life Sci. 349 (2016) 627–637.

[43] B. Mathew, G. Ucar, G.E. Mathew, M. Joy, K.E. Machaba, M.E.S. Soliman, Development of new class of thienylchalcones as hMAO-B inhibitors: synthesis, biochemistry and molecular dynamics studies, ChemistrySelect 2 (2017) 11113–11119.

[44] J. Suresh, S.C. Baek, S.P. Ramakrishnan, H. Kim, B. Mathew, Discovery of potent and reversible MAO-B inhibitors as furanochalcones, Int. J. Bio. Macromol. 108 (2018) 660–664.

[45] R. Sasidharan, S.C. Baek, S.L. Manju, H. Kim, B. Mathew, Imidazole bearing chalcones as new class of monoamine oxidase inhibitors, Biomed. Pharmacother. 106 (2018) 8–13.

[46] B. Mathew, S.C. Baek, D.G.T. Parambi, J.P. Lee, G.E. Mathew, S. Jayanthi, V. Devaraji, C. Raphaeal, V. Devikrishna, K.S. Shad, M.S. Uddin, H. Kim. Potent and highly selective dual-targeting monoamine oxidase-B inhibitors: Fluorinated chalcones of morpholine versus imidazole. Arch. Pharm. Chem. Life Sci. 2019;e1800309.

[47] R. Shalaby, J.P. Petzer, A. Petzer, U.A. Ashraf, E. Atari, F. Alasmari, S. Kumarasamy, Y. Sari, A. Khali, SAR and molecular mechanism studies of monoamine oxidase inhibition by selected chalcone analogs, J. Enzy. Inhib. Med. Chem. 34 (2019) 863–876.

[48] O.A. Chaves, B. Mathew, D.C. Sobrinho, B. Lakshminarayanan, M. Joy, G.E. Mathew, J. Suresh, J.C.N. Netto-Ferreira, Spectroscopic, zeta potential and molecular docking analysis on the interaction between human serum albumin and halogenated thienyl chalcones, J. Mol. Liq. 242 (2017) 1016–1026.

[49] O.A. Chaves, R. Sasidharan, C.H.C. dos Santos de Oliveria, S.L. Manju, M. Joy, B. Mathew B, J.C.N. Ferreira. In vitro study of the interaction between HSA and indolylchalcone, a potent human MAO-B inhibitor: spectroscopic and molecular modeling studies. ChemistrySelect. 4 (2019) 1007–1014.

[50] B. Mathew, A.A. Adeniyi, M. Joy, G.E. Mathew, A. Pillay, C. Sudarsanakumar, M.E.S. Soliman, Anti-oxidant behaviour of functionalized chalcone-a combined quantum chemical and crystallographic structural investigation, J. Mol. Stru. 1147 (2017) 682–696.

[51] L.J. Legoabe, A. Petzer, J.P. Petzer, The synthesis and evaluation of C7-substituted tetralone derivatives as inhibitors of monoamine oxidase, Chem. Biol. Drug Des. 86 (2015) 895–904.

[52] S.-Y. Son, J. Ma, Y. Kondou, M. Yoshimura, E. Yamashita, T. Tsukihara, Structure of human monoamine oxidase A at 2.2-A resolution: the control of opening the entry for substrates/inhibitors, Proceedings of the National Academy of Sciences 105 (15) (2008) 5739–5744, https://doi.org/10.1073/pnas.0710626105.

[53] C. Binda, J. Wang, L. Pisani, C. Caccia, A. Carotti, P. Salvati, D.E. Edmondson, A. Mattevi, Structures of human monoamine oxidase B complexes with selective noncovalent inhibitors: safinamide and coumarin analogs, J. Med. Chem. 50 (2007) 5848–5852.

[54] Schrödinger Release 2018-2: QikProp, Schrödinger, LLC, New York, NY, 2018.

[55] B. Mathew, S.C. Baek, D.G.T. Parambi, P. Lee, M. Joy, R. Annie, R.V. Randev, P. Nithyamol, V. Vijayan, S.T. Inasu, G.E. Mathew, K.K. Lohidakshan, G.K. Krishnan, H. Kim, Selected aryl thiosemicarbazones as a new class of multi-targeted monoamine oxidase inhibitors, Med. Chem. Comm. 9 (2018) 1871–1881.

[56] H.W. Lee, H.W. Ryu, M.G. Kang, D. Park, S.R. Oh, H. Kim, Potent selective monoamine oxidase B inhibition by maackiain, a pterocarpan from the roots of Sophora flavescens, Bioorg. Med. Chem. Lett. 26 (2016) 4714–4719.

[57] S.C. Baek, H.W. Lee, H.W. Ryu, M.G. Kang, D. Park, S.H. Kim, M.L. Cho, S.R. Oh, H. Kim, Selective inhibition of monoamine oxidase A by hispidol, Bioorg. Med. Chem. Lett. 15 (2018) 584–588.

[58] Schrödinger Release 2018-2: Schrödinger Suite 2018-2 Protein Preparation Wizard.

[59] Schrödinger Release 2018-2: Schrödinger Suite 2018-2 QM-Polarized Ligand Docking protocol.

[60] Schrödinger Release 2018-2: Glide, Schrödinger, LLC, New York, NY.

[61] U. Ryde Genheden, The MM/PBSA and MM/GBSA methods to estimate ligand-binding affinities, Expert Opin. Drug. Discov. 10 (2015) 449–461.